Evolution Between Exciton and Exciplex Emission in Planar Heterojunction OLEDs with Different Hole-Injection Characteristics

Xi Zhao, Jing Chen, Yuting Wu, Fuxian Wei, Huiyao Wang, Xiaoli Chen, and Zuhong Xiong*
Chongqing Key Laboratory of Micro&Nano Structure Optoelectronics, School of Physical Science and Technology, Southwest University, Chongqing 400715, China

(Received 10 October 2022; revised 24 March 2023; accepted 24 April 2023; published 22 May 2023)

Planar heterojunction-based organic light-emitting diodes (PHJ OLEDs) usually have simultaneous exciton and exciplex emissions and understanding their evolution processes is crucial for designing high-performance white OLEDs, but relevant evolution mechanisms are still unclear. Here, unreported competitions between exciton and exciplex emissions and an undiscovered energy-transfer channel from triplet exciton to triplet exciplex states in PHJ OLEDs with different hole-injection abilities are investigated by separately measuring their current-dependent electroluminescence (EL) spectra and magneto-EL (MEL) traces at different temperatures. Interestingly, the ratio of emission intensity between exciton and exciplex states ($R = I_{\text{exciton}}/I_{\text{exciplex}}$) from the device with a good hole-injection ability rises with increasing bias current at each temperature, whereas that from the device with a poor hole-injection ability hardly changes. In addition, R from the devices with good and poor hole-injection abilities show nonmonotonic variation and monotonic reduction with decreasing operational temperature at each bias current, respectively. These various current- and temperature-dependent competitions between exciton and exciplex emissions are attributed to distinct current- and temperature-dependent electron-tunneling effects occurring at organic heterojunction interfaces of devices with different hole-injection abilities. More intriguingly, using MEL as a fingerprint detection tool, we find there is a Dexter energy-transfer (DET) channel from the triplet exciton to triplet exciplex ($T_1 \rightarrow EX_3$) state and the DET can enhance the reverse intersystem crossing (RISC) process from triplet to singlet exciplexes ($EX_3 \rightarrow EX_1$), which cannot be found using the conventional probing tool, EL spectra. Because the numbers of T_1 excitons in these devices have different current and temperature dependencies, various current- and temperature-dependent DET and RISC processes happen, which cause abundant MEL behaviors. Obviously, this work deepens the physical understanding of the competition and DET processes between exciton and exciplex states in PHJ OLEDs.

DOI: 10.1103/PhysRevApplied.19.054067

I. INTRODUCTION

Exciton and exciplex emissions are often generated simultaneously from planar heterojunction-based organic light-emitting diodes (PHJ OLEDs) and their evolution processes need to be well understood to improve the color purity and the quantum efficiency of white OLEDs [1–3]. As has been well reported, relevant evolution processes are usually discussed by measuring and analyzing electroluminescence (EL) spectra of PHJ OLEDs [4–8]. For example, Zhang *et al.* used EL spectra to discover that poly(N-vinylcarbazole) (PVK) exciton and PVK/(2-(4-biphenylyl)-5-(4-tert-butylphenyl)-1,3,4-oxadiazole (PBD) exciplex emissions arise simultaneously from the PVK/PBD PHJ OLED and the ratio of emission intensity between exciton and exciplex states ($R = I_{\text{exciton}}/I_{\text{exciplex}}$) reduces with increasing device bias voltage [4]. He *et al.* employed EL spectra to find that the N,N′-diphenyl-N,N′-bis(1,1′-biphenyl)-4,4′-diamine (NPB)/2-phenyl-4,6-bis(3,5-di-4-pyridylphenyl) pyrimidine (B4PyPPM) PHJ OLED has simultaneous NPB exciton and NPB/B4PyPPM exciplex emissions and R reduces with increasing the B4PyPPM layer thickness [5]. Nishikitani *et al.* utilized EL spectra to observe that poly(9,9-di-n-dodecylfluorenyl-2,7-diyl) (PFD) exciton and poly(4-methyl-triphenylamine-co-acetoaldehyde) (TPA-AA)/PFD exciplex emissions are produced simultaneously from the TPA-AA/PFD PHJ OLED and R rises when the device electron-injection ability is improved by inserting the electron-injection layer between the PFD layer and the Al cathode [6]. Although some consensus for the evolution processes of exciton and exciplex emissions has been reached, these evolution processes need further extensive research because they depend significantly on

*zhxiong@swu.edu.cn

the architecture parameter, the bias voltage, or the operational temperature of the devices [4–8].

Furthermore, many studies show that triplet excitons (T_1) usually have higher energy levels than triplet exciplexes (EX_3) [9], which indicates that the Dexter energy-transfer (DET) channel from T_1 to EX_3 ($T_1 \rightarrow EX_3$) may be present in PHJ OLEDs. Note that this DET can increase the quantity of EX_3 and therefore enhance the reverse intersystem crossing (RISC) process from triplet to singlet exciplexes ($EX_3 \rightarrow EX_1$). Then, the increased number of EX_1 will enhance the exciplex emission and change the device light color, although the exciton utilization efficiencies are improved. Obviously, discovering the DET channel is important for recognizing the evolution processes of exciton and exciplex states. However, this DET has seldom been reported in the literature due to the absence of the exciplex absorption spectrum. Specifically, DET requires the spectral overlap between the exciton emission spectrum and exciplex absorption spectrum [10]. Unfortunately, there is no exciplex absorption spectrum. This is because exciplexes, whose holes and electrons are located on highest occupied molecular orbitals (HOMOs) of electron-donor molecules and lowest unoccupied molecular orbitals (LUMOs) of electron-acceptor molecules, respectively, are always formed in excited states and they do not exist in ground states [10]. Thus, searching for a feasible way to find this DET channel from triplet excitons to exciplexes is necessary.

Herein, unreported competitions between NPB exciton and NPB/2,4,6-tris[3-(diphenylphosphinyl)phenyl]-1,3,5-triazine (PO-T2T) exciplex emissions and an undiscovered DET channel from triplet NPB exciton to triplet NPB/PO-T2T exciplex states are discussed by measuring current- and temperature-dependent EL spectra and magneto-EL (MEL) traces from NPB/PO-T2T PHJ OLEDs with different hole-injection abilities. Specifically, the R of $I_{exciton}$ to $I_{exciplex}$ from the device with a poor hole-injection ability hardly changes with the bias current at each temperature, but reduces as the temperature decreases at each bias current. Surprisingly, after improving the device hole-injection ability by modifying the hole-injection layer, R rises with increasing bias current at each temperature and first increases but then reduces with decreasing temperature at each bias current. These various current- and temperature-dependent competitions between exciton and exciplex emissions are induced by distinct current and temperature dependencies of the electron-tunneling effects happening at the NPB/PO-T2T interfaces of the devices with different hole-injection abilities. More surprisingly, we use MEL as a fingerprint probing tool to discover that there is a DET channel from T_1 excitons to EX_3 states ($T_1 \rightarrow EX_3$), which cannot be found using the usual detection technique of EL spectra. In addition, this DET can increase the number of EX_3 states and therefore enhance the RISC process from EX_3 to EX_1 ($EX_3 \rightarrow EX_1$). According to the current-dependent EL spectra of these devices at different temperatures, the quantities of T_1 excitons have different current and temperature dependencies, which induce various current- and temperature-dependent DET and RISC processes and abundant MEL behaviors. Clearly, this work enriches the full understanding of the competition and DET processes between exciton and exciplex states in PHJ OLEDs.

II. EXPERIMENTAL SECTION

Three kinds of NPB/PO-T2T PHJ OLEDs with different hole-injection abilities are fabricated as follows. Device 1 (dev 1) has the device architecture of ITO/1,4,5,8,9,11-hexaaza-triphenylene-hexacarbonitrile (HAT-CN)(20 nm)/NPB(80 nm)/PO-T2T(80 nm)/LiF(1 nm)/Al(120 nm). Device 2 (dev 2) is ITO/NPB(80 nm)/PO-T2T(80 nm)/LiF (1 nm)/Al(120 nm). Device 3 (dev 3) uses poly(3,4-ethylenedioxythiophene):poly(styrenesulfonate) (PEDOT:PSS) instead of HAT-CN used in dev 1 That is, dev 3 is ITO/PEDOT:PSS(40 nm)/NPB(80 nm)/PO-T2T(80 nm)/LiF(1 nm)/Al(120 nm). In addition, the pure exciplex-emission reference device (RD) used for comparison has the following structure: ITO/HAT-CN(20 nm)/NPB(40 nm)/NPB:PO-T2T(80 nm)/PO-T2T (40 nm)/LiF(1 nm)/Al(120 nm). For device fabrication, the PEDOT:PSS layer is first spin-coated onto the substrate and then annealed for 10 min at 120 °C in a vacuum chamber. The other organic functional layers and LiF/Al cathode are grown using the multiple-source organic molecular beam deposition system under high vacuum (base pressure of approximately 10^{-6} Pa) at growth rates of 0.1–0.5 Å/s. To monitor the growth rate and the thickness of these functional layers, a calibrated quartz crystal oscillator controlled by an XTM/2 unit is placed close to the sample holder.

For device measurements, freshly prepared samples are mounted on the cold finger of a closed-cycle cryostat (Janis: CCS-350S). The sample temperatures are set with the use of the temperature controller (Lakeshore 331). The external magnetic field B is applied by an electromagnet (Lakeshore EM647) and measured using a Hall probe gaussmeter placed close to the sample. A Keithley 2400 SourceMeter is used to provide the bias voltage and record current signals at the same time. A Keithley 2000 multimeter connected with a silicon photodetector is employed to record the device EL brightness. The device EL spectra are tested using a Princeton spectrometer (Acton SpectraPro 2300i) once the Keithley 2400 SourceMeter supplies a constant voltage to the device to obtain a certain EL intensity. Photoluminescence (PL) spectra and transient PL decay of thin films are measured with an Edinburgh fluorescence spectrometer (FLS1000).

III. RESULTS AND DISCUSSION

A. Energy-level structures and photoelectric properties of dev 1 and dev 2

As shown in Figs. 1(a) and 1(b), dev 1 and dev 2 are NPB/PO-T2T PHJ OLEDs with and without a HAT-CN/NPB heterojunction charge-generation unit, respectively. NPB and PO-T2T are hole- and electron-transporting materials, respectively, and their chemical molecular structures are displayed in Fig. 1(c). Interestingly, although dev 1 and dev 2 have similar device structures, they emit two different colors of light at the same bias current. These two distinct emission colors can be expressed by their different chromaticity coordinates, which are (0.44, 0.37) and (0.25, 0.24), respectively, on the Commission International de I'Eclairage chromaticity diagram (Fig. S1 in the Supplemental Material [11]). To explain the different emission colors from dev 1 and dev 2, PL spectra of the pure NPB and PO-T2T films and the NPB:PO-T2T codeposited film are measured and shown in Fig. 1(d). As can be seen, the PL spectrum from the NPB:PO-T2T film exhibits a double-peak emission. The short-wavelength peak (around 437 nm) is consistent with the PL peak (around 435 nm) from the NPB film, which confirms the presence of NPB exciton states. The long-wavelength peak (about 589 nm) is broad and red-shifted relative to the PL peaks (around 435 and 395 nm) from the NPB and PO-T2T films, which proves the formation of NPB:PO-T2T exciplex states. So, the short- and long-wavelength peaks in the PL spectrum of the NPB:PO-T2T film originate from the NPB exciton and NPB:PO-T2T exciplex emissions, respectively. Next, EL spectra of dev 1 and dev 2 are measured at the bias current of 50 μA as shown in Fig. 1(e). As can be seen, their EL spectra also present double-peak emissions. By comparing the EL spectra of dev 1 and dev 2 with the PL spectrum of the NPB:PO-T2T film, it can be concluded that the short- and long-wavelength peaks (around 436 and 590 nm) in their EL spectra also separately exhibit the NPB exciton and NPB/PO-T2T exciplex emissions.

Note that, although both the EL spectra of dev 1 and dev 2 are composed of the exciton and exciplex emissions, their main EL emissions are different [Fig. 1(e)]. Specifically, the EL spectrum of dev 1 is dominated by the exciplex emission, but that of dev 2 is governed by the exciton emission. That is, distinct emission colors from dev 1 and dev 2 are induced by different competitions between exciton and exciplex emissions from these two devices. These two distinct competitions can be explained by comparing different locations of the electron-hole recombination zone in dev 1 and dev 2, which are determined by various charge balances at the NPB/PO-T2T interface of these two devices. In dev 1, electrons injected from the LiF/Al cathode and holes generated at the HAT-CN/NPB interface initially hop towards each other under the external electric field and accumulate at the NPB/PO-T2T interface [Fig. 1(a)]. These charge carriers are electron-rich, i.e., the number of electrons is more than that of holes. This is because the electron-injection ability of dev 1 is stronger than its hole-injection ability.

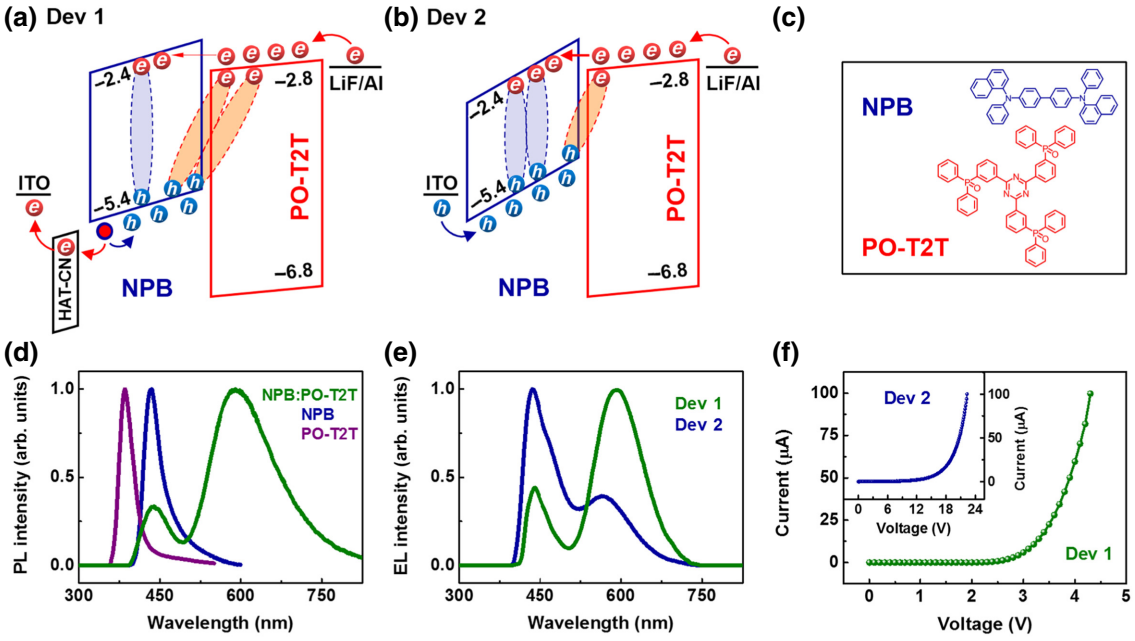

FIG. 1. (a),(b) Energy-level diagrams of dev 1 and dev 2. (c) Chemical molecular structures of NPB and PO-T2T. (d) Normalized PL spectra of pure NPB and PO-T2T films and the NPB:PO-T2T codeposited film. (e) Normalized EL spectra of dev 1 and dev 2 at the bias current of 50 μA. (f) Current-voltage characteristics of dev 1 and dev 2 at 300 K.

Specifically, the electron-injection barrier (0.1 eV) from the LiF/Al cathode to the LUMO of PO-T2T is lower than the hole-injection barrier (0.3 eV) from the LUMO of HAT-CN to the HOMO of NPB. Moreover, the electron mobility (10^{-3} cm^2 V^{-1} s^{-1}) of PO-T2T [12] is higher than the hole mobility (10^{-4} cm^2 V^{-1} s^{-1}) of NPB [13]. This indicates that a small proportion of electrons tunnel from the LUMO of PO-T2T to the LUMO of NPB, which means most electrons stay at the NPB/PO-T2T interface. That is, a small proportion of electrons and holes recombine within the NPB layer to generate exciton states, whereas most of them recombine at the NPB/PO-T2T interface to form exciplex states. Thus, the EL spectrum of dev 1 is dominated by the exciplex emission.

In sharp contrast to dev 1, dev 2 has no HAT-CN/NPB heterojunction charge-generation unit [Figs. 1(a) and 1(b)], which increases the hole-injection barrier and turn-on voltage [Fig. 1(f)]. Specifically, the hole-injection barrier (0.6 eV) from the ITO anode to the HOMO of NPB in dev 2 is larger than that (0.3 eV) from the LUMO of HAT-CN to the HOMO of NPB in dev 1. This indicates that the hole-injection ability of dev 2 is weaker than that of dev 1. Meanwhile, because the hole-injection ability of dev 1 is weaker than its electron-injection ability and dev 1 and dev 2 have same electron-injection abilities, the hole-injection ability of dev 2 is much weaker than its electron-injection ability. That is, the charge carriers at the NPB/PO-T2T interface in dev 2 are relatively unbalanced compared to those in dev 1, which can be proved by the lower current efficiency of EL from dev 2 than in dev 1 (Fig. S2 in the Supplemental Material [11]). Since the number of holes at the NPB/PO-T2T interface in dev 2 is much lower than that of electrons, fewer electrons stay at this interface, while most electrons tunnel from the LUMO of PO-T2T to the LUMO of NPB. That is, only a small proportion of electrons and holes recombine at the NPB/PO-T2T interface to form exciplex states, and most of them recombine within the NPB layer to produce exciton states. Hence, the EL spectrum of dev 2 is governed by the exciton emission.

B. Current-dependent EL spectra of dev 1 and 2 at different temperatures

To further study the competitions between exciton and exciplex emissions from dev 1 and dev 2, their current-dependent EL spectra are measured at different temperatures and normalized according to the exciplex emission intensity as shown in Figs. 2 and 3, respectively. Obviously, these EL spectra have various current and temperature dependencies. To quantitatively discuss the current-dependent EL spectra of dev 1 and dev 2, the ratio between exciton and exciplex emissions is expressed as $R = I_{\text{exciton}}/I_{\text{exciplex}}$, and R values for these two devices at 300 K as a function of the bias current are summarized in Figs. 4(a) and 4(b), respectively. Interestingly, although dev 1 and dev 2 have similar structures, R values for these two devices show different current dependencies. Specifically, R from dev 1 rises with increasing bias current, whereas that from dev 2 hardly changes. These two distinct current-dependent R behaviors can be explained by analyzing different current dependencies of the electron-tunneling process occurring at the NPB/PO-T2T interface in dev 1 and dev 2. As well reported in the literature [14,15], the electron-tunneling process is determined by the transmission coefficient (TC) that often first rises but then saturates with reducing barrier width. That is, the TC rises with reducing barrier width when the barrier is wide, but the TC hardly changes when it is narrow. Because the barrier width of the electron injection at the NPB/PO-T2T interface in dev 1 is wide owing to the slight band bending of the NPB layer [Fig. 1(a)], the TC rises with the reduction of the barrier width. Note that improving the bias current of dev 1 reduces this barrier width, leading to the increased TC. This is because the increase in the bias current is achieved by improving the device bias voltage. When the device bias voltage rises, the bias voltage on the NPB layer elevates, which enhances the electric field within the NPB layer and promotes its band bending. So, the barrier width of the electron injection at the NPB/PO-T2T interface reduces, resulting in the increased TC and enhanced electron-tunneling process. This means that the quantity of electrons within the NPB layer rises but the number of electrons at the NPB/PO-T2T interface reduces, i.e., the formation of exciton states is facilitated but exciplex states are difficult to produce. Thus, the R of I_{exciton} to I_{exciplex} from dev 1 at 300 K rises as the bias current increases. Consistent with current-dependent EL spectra of dev 1 at 300 K, those measured at 250, 200, 150, 100, and 20 K also indicate that R rises with increasing bias current [Figs. 2(b)–2(f)], which is verified by the current-dependent EL spectra of dev 3 with a similar hole-injection ability (Text S1, Figs. S4 and S5 in the Supplemental Material [11]).

Then, the current-independent R from dev 2 is explained by analyzing the current dependence of the electron-tunneling process occurring at the NPB/PO-T2T interface. As mentioned previously, the TC of the electron tunneling hardly changes with the narrow barrier width. Because the barrier width of the electron injection at the NPB/PO-T2T interface in dev 2 is narrow due to the sharp band bending of the NPB layer [Fig. 1(b)], the reduction of the barrier width hardly increases the TC. When the TC is constant, the injected electrons at different bias currents are distributed in a fixed ratio between the NPB layer and the NPB/PO-T2T interface. This indicates that the ratio of exciton to exciplex states is constant at different bias currents. Thus, R for dev 2 at 300 K is insensitive to the bias current, which is further explained by simulating the electron-hole recombination zones in dev 2 at different bias currents using the SIMOLED simulation software [16,17]

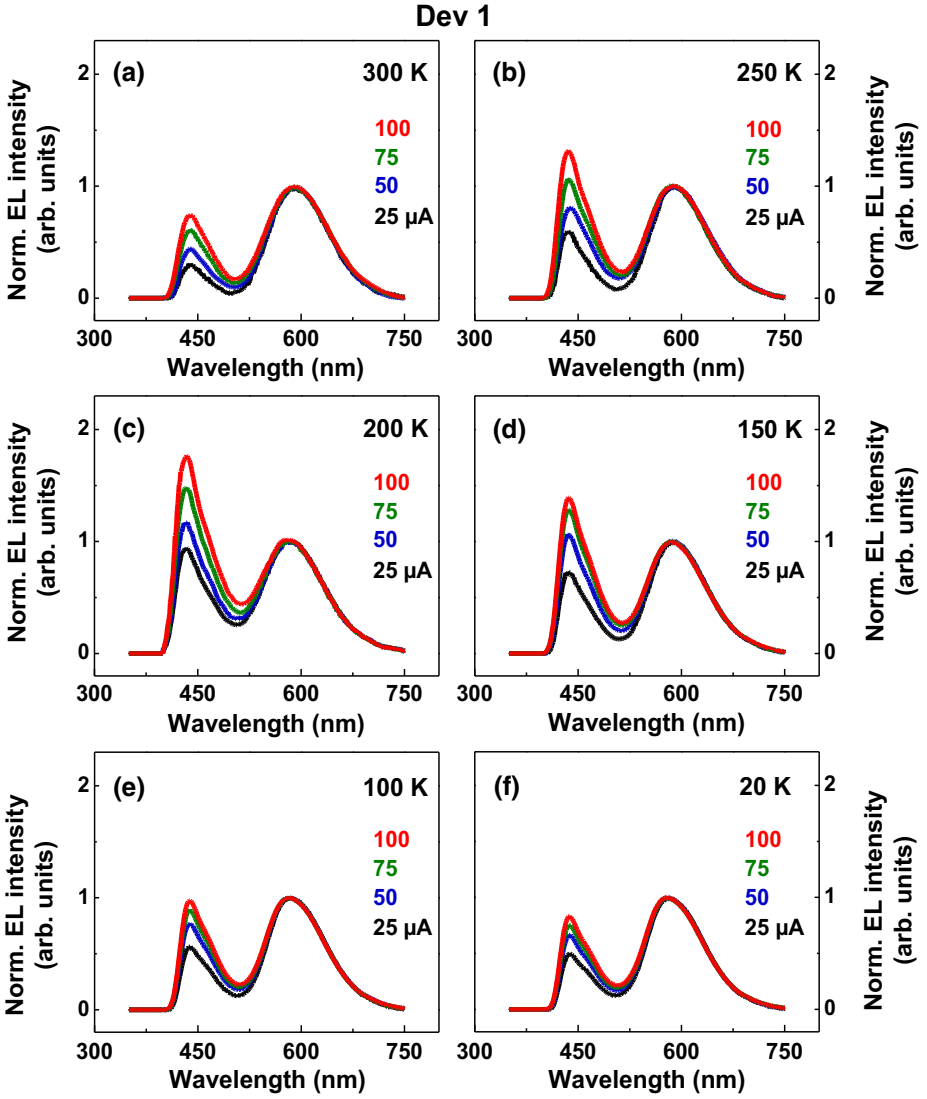

FIG. 2. (a)–(f) Current-dependent EL spectra of dev 1 at different temperatures.

for organic photoelectric devices, as stated in Text S2 and Fig. S6 within the Supplemental Material [11]. Similar to current-dependent EL spectra of dev 2 at 300 K, those obtained at 250, 200, 150, 100, and 20 K also reflect that R has no current dependencies [Figs. 3(b)–3(f)].

Next, temperature-dependent competitions between exciton and exciplex emissions from dev 1 and dev 2 are investigated by quantitatively analyzing their temperature-dependent EL spectra (Figs. 2 and 3). Specifically, R values from dev 1 and dev 2 at the bias current of 100 μA as a function of temperature are summarized in Figs. 4(c) and 4(d), respectively. As can be seen, R values from these two devices have different temperature dependencies. That is, R from dev 1 shows nonmonotonic variation, which first rises and then reduces with decreasing the temperature, but that from dev 2 displays monotonic reduction. These two distinct temperature-dependent R behaviors can be explained by analyzing different temperature dependencies of the electron-tunneling process occurring at the NPB/PO-T2T interface in dev 1 and dev 2. As mentioned previously, the TC of the electron tunneling at the NPB/PO-T2T interface in dev 1 rises when the wide barrier width is reduced. Clearly, decreasing the operational temperature of dev 1 reduces this barrier width and thus the TC rises. This is because the device bias voltage at a fixed bias current rises with decreasing temperature, as shown in Fig. S3(a) within the Supplemental Material [11]. When the device bias voltage rises, the bias voltage on the NPB layer increases, which enhances the electric field within the NPB layer and facilitates the band bending of the NPB layer. So, the barrier width of the electron injection at the NPB/PO-T2T interface reduces and the TC rises. Furthermore, note that the TC of the electron tunneling is affected not only by the barrier width, but also by the environmental heat. It is well

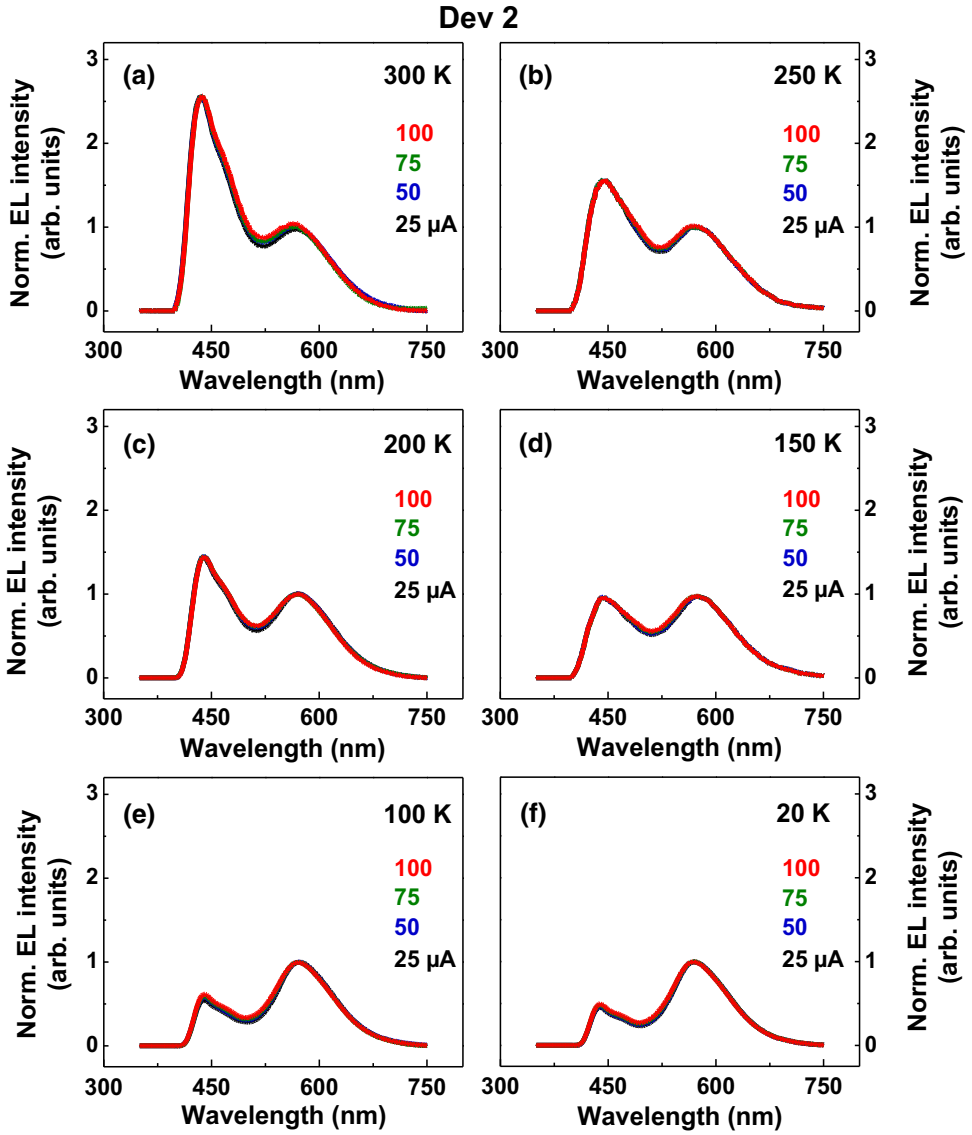

FIG. 3. (a)–(f) Current-dependent EL spectra of dev 2 at different temperatures.

reported that the TC reduces with decreasing temperature. This is because electron tunneling is an endothermic process, but the environmental heat reduces as the temperature decreases [13,18]. Obviously, the reduced barrier width and the decreased environmental heat produce opposite effects on the TC and they compete with each other as the temperature decreases. Specifically, when the temperature decreases from 300 to 200 K, because the environmental heat drops slightly, the TC is dominated by the reduced barrier width, i.e., the TC rises. However, as the temperature further decreases from 200 to 20 K, since the environmental heat drops significantly, the TC is governed by the decreased environmental heat, i.e., the TC reduces. So, the TC first rises but then reduces (i.e., the electron-tunneling process first enhances but then weakens) when decreasing the temperature from 300 to 20 K [Fig. 5(a)]. This reflects that the quantity of electrons within the NPB layer first rises and then reduces, while the number of electrons at the NPB/PO-T2T interface first reduces and then rises. Hence, the R of I_{exciton} to I_{exciplex} from dev 1 first rises and then reduces as the temperature decreases, which has been examined using the temperature-dependent EL spectra of dev 3 with a similar hole-injection ability, as described in Text S1.

Then, the monotonically decreasing R from dev 2 with decreasing temperature is explained by discussing its temperature-dependent electron-tunneling process occurring at the NPB/PO-T2T interface. As stated previously, the TC of the electron tunneling is determined by the competition between the reduced barrier width and the decreased environmental heat while the temperature is reduced. Because the TC at the NPB/PO-T2T interface in

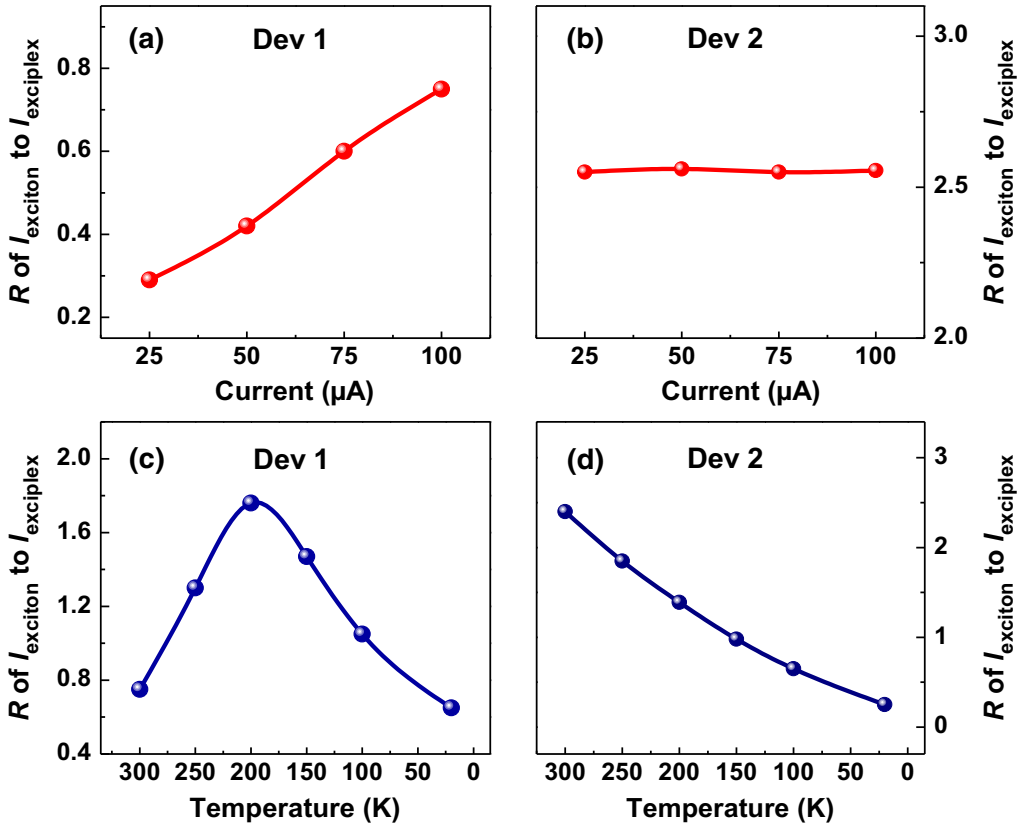

FIG. 4. (a),(b) R of I_{exciton} to I_{exciplex} from dev 1 and dev 2 at 300 K as a function of the bias current. (c),(d) R at the bias current of 100 μA as a function of the temperature.

dev 2 hardly changes with its narrow barrier width, the TC is dominated by the decreased environmental heat. This indicates that the TC reduces and the electron-tunneling process weakens with decreasing temperature [Fig. 5(b)]. That is, the quantity of electrons within the NPB layer reduces but the number of electrons at the NPB/PO-T2T interface rises, which impedes the formation of excitons within the NPB layer, but facilitates that of exciplexes at the NPB/PO-T2T interface. Thus, the R of I_{exciton} to I_{exciplex} from dev 2 reduces as the temperature decreases, which is further explained by simulating the electron-hole recombination zones in dev 2 at different temperatures as stated in Text S2 within the Supplemental Material [11]. In a word, we use EL spectra to investigate various current- and temperature-dependent competitions between exciton and exciplex emissions from dev 1 and dev 2, which are caused by different current and temperature dependencies of the electron-tunneling process occurring at the NPB/PO-T2T interface of these two devices.

C. Current-dependent MEL traces of dev 1, dev 2, and RD at 300 K

Although the competitions between exciton and exciplex emissions from dev 1 and dev 2 are discussed by measuring their EL spectra, the interaction processes between exciton and exciplex states need further research owing to the limitation of the EL probing tool. For example, the interaction processes of exciton and exciplex states usually influence their physical microscopic channels, including intersystem crossing (ISC) and RISC between EX_1 and EX_3 [19], triplet-triplet annihilation (TTA, $T_1 + T_1 \rightarrow S_1 + S_0$) of T_1 excitons [20–22], and triplet-charge annihilation (TQA) between triplet states and excessive charge carriers [23,24]. However, the conventional EL detection tool (e.g., the EL spectra) cannot identify these microscopic processes. Recently, using MEL as a fingerprint probing tool to visualize the physical microscopic processes of exciton and exciplex states has gained increasing attention because these processes are highly spin dependent and have characteristic MEL traces [19–24], as shown in Fig. S7 within the Supplemental Material [11]. For instance, the ISC and RISC processes produce characteristic MEL traces that, respectively, display inverted and upright Lorentzian-type line shapes with typical linewidths of several millitesla [19, 24]. Thus, to study the interaction processes between exciton and exciplex states in dev 1 and dev 2, their current- and temperature-dependent MEL traces are measured, as shown in Figs. 6(a), 6(b), 7(a), and 7(b), respectively. Furthermore, to better understand these MEL traces, RD with a single exciplex-emission is fabricated (Fig. S8 in the Supplemental Material [11]) and its current- and temperature-dependent MEL traces are used for comparison [Figs. 6(c) and 7(c)]. As for the single exciplex emission from RD, it can be proved by the solely broad and

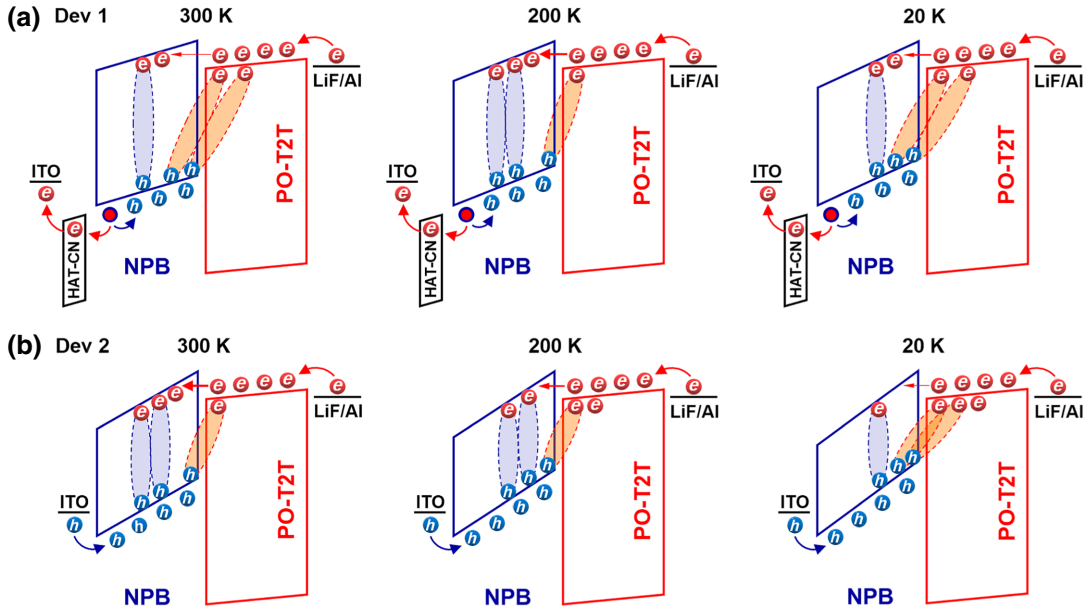

FIG. 5. Tunneling and recombination processes of charge carriers at the NPB/PO-T2T interfaces in (a) dev 1 and (b) dev 2 at 300, 200, and 20 K.

red-shifted EL peaks (around 593 nm) from RD relative to the PL peaks (around 435 and 395 nm) from the NPB and PO-T2T films.

We first investigate the current-dependent MEL traces of dev 1, dev 2, and RD at 300 K [Figs. 6(a)–6(c)]. MEL is defined as the relative change in the EL intensity upon the application of an external B [19–24], that is,

$$\mathrm{MEL} = \frac{\mathrm{EL}(B) - \mathrm{EL}(0)}{\mathrm{EL}(0)} \times 100\% \tag{1}$$

where EL(B) and EL(0) are the EL intensities with and without the external B, respectively. As can be seen, MEL traces of RD at all bias currents present sharply increasing low-field effects (LFEs, $|B| \leq 10$ mT) and slowly rising high-field effects (HFEs, $30 < |B| \leq 300$ mT). The B ranges of LFEs and HFEs are acquired by fitting the MEL traces of RD using a reported empirical formula [24,25], which is expressed by Eq. (2) in the following. According to the fingerprint MEL traces (Fig. S7 in the Supplemental Material [11]), LFEs and HFEs of RD are separately attributed to the B-suppressed ISC from singlet to triplet polaron pairs ($\mathrm{PP}_1 \rightarrow \mathrm{PP}_3$) and TQA processes. Similar to the LFEs and HFEs of RD, those of dev 2 at all bias currents also display the B-suppressed ISC and TQA, respectively. It is well reported that MEL traces of PHJ OLEDs often exhibit only LFEs and HFEs [26,27]. Surprisingly, in addition to LFEs and HFEs, MEL traces of dev 2 at all bias currents still present rapidly decreasing intermediate-field effects (IFEs, $10 < |B| \leq 30$ mT), which have not been previously observed from PHJ OLEDs. The B range of IFEs is obtained by fitting the MEL traces of dev 2 using Eq. (2).

More surprisingly, although the MEL trace of dev 1 at the small bias current of 25 μA solely shows LFE and HFE, rapidly decreasing IFE gradually appears when increasing the bias current from 25 to 100 μA. At the large bias current of 100 μA, only IFE and HFE are observed from dev 1 since the IFE and HFE of dev 1 are far stronger than its LFE. According to the characteristic MEL traces in Fig. S7 within the Supplemental Material [11], IFEs of dev 1 and dev 2 are attributed to the B-mediated RISC process from EX_3 to EX_1 ($\mathrm{EX}_3 \rightarrow \mathrm{EX}_1$), which is explained in detail in Fig. 8.

To quantitatively analyze current-dependent ISC, RISC, and TQA processes in dev 1, dev 2, and RD, their current-dependent MEL traces are fitted by Eq. (2). Equation (2) contains two Lorentzian functions and a non-Lorentzian function, which can be expressed as follows:

$$\mathrm{MEL} = C_1 \frac{B^2}{B^2 + B_1^2} - C_2 \frac{B^2}{B^2 + B_2^2} + C_3 \frac{B^2}{(|B| + B_3)^2}. \tag{2}$$

Empirical Lorentzian and non-Lorentzian functions are often used to separately fit LFEs and HFEs of MEL traces to analyze their formation mechanisms [24,25,28]. This is because various physical microscopic processes of spin-pair states simultaneously occur in a device and the MEL trace of the device is a superposition of MEL behaviors for these processes. That is, Eq. (2) can be used to fit and decompose the MEL trace to analyze different occurrence magnitudes of these microscopic physical processes. In Eq. (2), these three terms model ISC, RISC, and TQA processes; B is the external magnetic field; B_1 (∼5 mT),

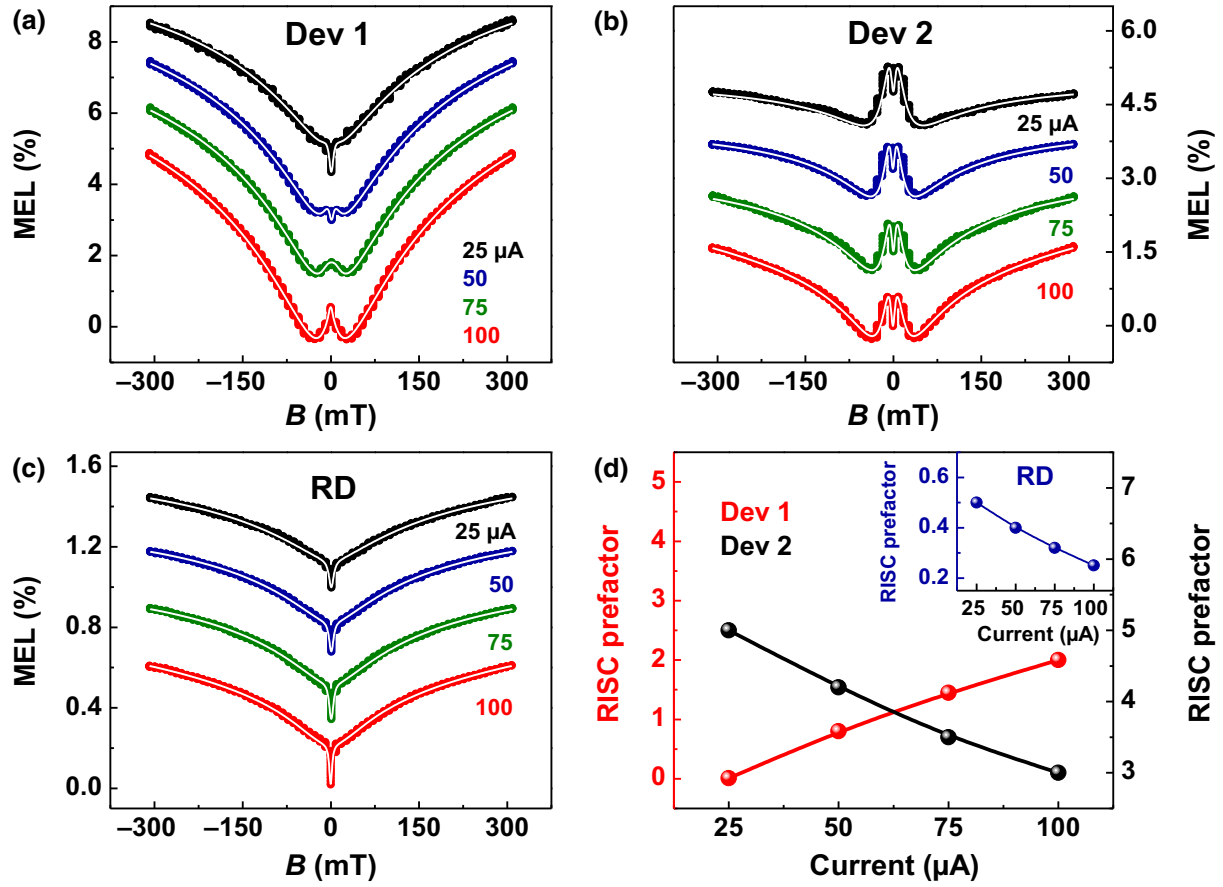

FIG. 6. (a)–(c) Current-dependent MEL traces of dev 1, dev 2, and RD and their fitted curves (white solid lines) at 300 K. (d) Prefactors used to describe the occurrence magnitudes of the RISC processes in these three devices at 300 K for different bias currents.

B_2 (∼10 mT), and B_3 (∼100 mT) are the characteristic scales of B for ISC, RISC, and TQA; and C_1, C_2, and C_3 are prefactors for describing the occurrence magnitudes of ISC, RISC, and TQA, respectively. As exhibited in Figs. 6(a)–6(c), the fitted curves (white solid lines) are in good agreement with the experimental data of dev 1, dev 2, and RD, and their prefactors C_1, C_2, and C_3 acquired at different bias currents are summarized in Figs. 6(d) and S9 within the Supplemental Material [11], respectively. As can be seen, the ISC and TQA processes in dev 1, dev 2, and RD have the same current dependencies. Specifically, TQA in these three devices enhances as the bias current rises due to the increased quantity of charge carriers. Furthermore, ISC in these three devices weakens with increasing bias current. This is because the increase in the bias current is achieved by improving the device bias voltage. When the bias voltage rises, the electric field inside the device increases, which enhances the field-induced dissociation of PP states and reduces their lifetimes according to the Onsager theory [29,30]. That is, the number of PP states that can undergo ISC reduces as the bias current increases, resulting in the weakened ISC. Although ISC and TQA in dev 1, dev 2, and RD have the same current dependencies, the RISC processes in these three devices show different current dependencies [Fig. 6(d)]. Specifically, RISC in dev 1 enhances as the bias current increases, whereas those in dev 2 and RD weaken. These different current-dependent RISCs are explained in detail in Fig. 8.

D. Temperature-dependent MEL traces of dev 1, dev 2, and RD at the bias current of 100 μA

Next, temperature-dependent MEL traces of dev 1, dev 2, and RD at the bias current of 100 μA are discussed to further study the interaction processes between exciton and exciplex states [Figs. 7(a)–7(c)]. As can be seen, LFEs and HFEs of RD at each temperature display the B-suppressed ISC and TQA processes, respectively. Although LFEs of dev 2 at each temperature also present the B-suppressed ISC, its IFEs and HFEs change significantly with the temperature. Specifically, the IFE of dev 2 at 300 K exhibits the B-suppressed RISC process but its IFE gradually disappears as the temperature decreases from 300 to 20 K. In addition, the HFE of dev 2 at 300 K displays the B-suppressed TQA process but this HFE converts from a slow rise to a slow decline with decreasing

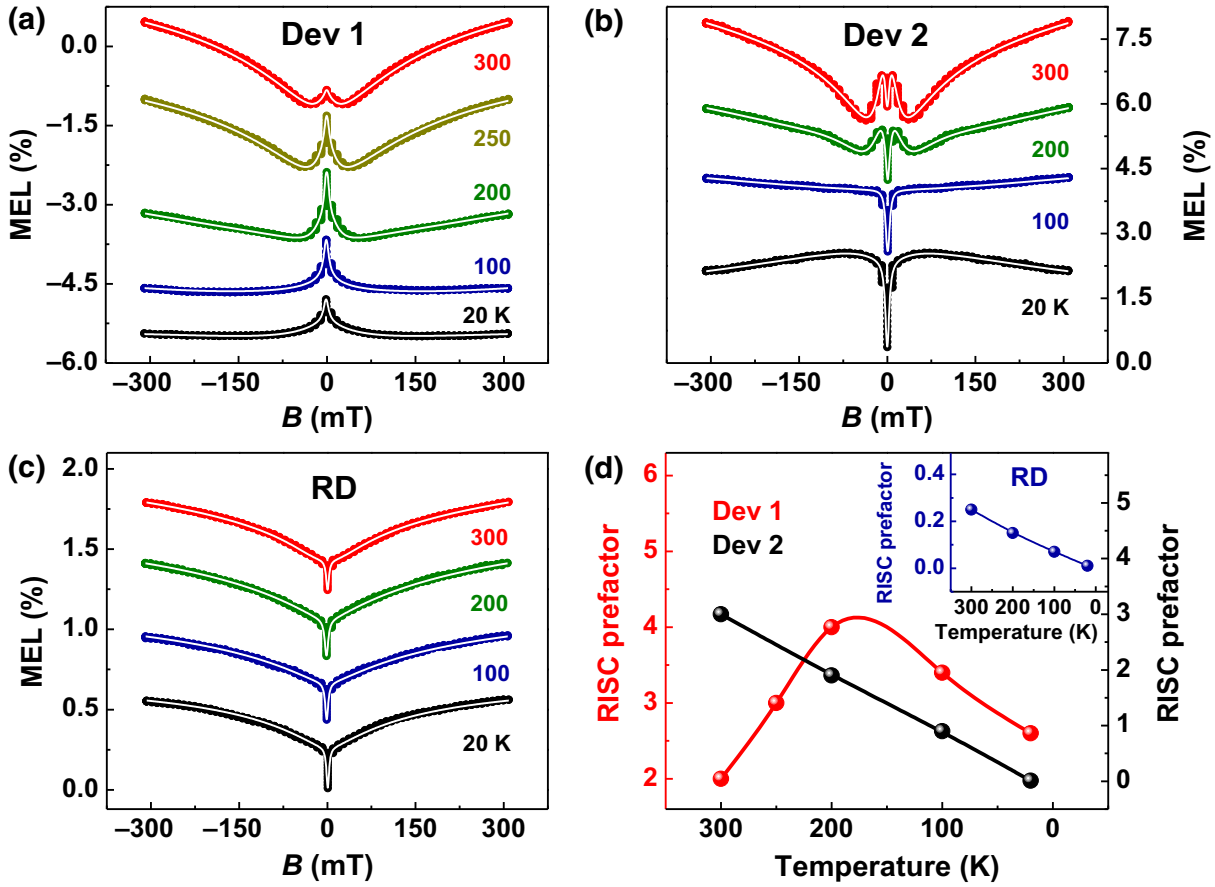

FIG. 7. (a)–(c) Temperature-dependent MEL traces of dev 1, dev 2, and RD and their fitted curves (white solid lines) at the bias current of 100 μA. (d) Prefactors for describing the occurrence magnitudes of the RISC processes in these three devices at the bias current of 100 μA for different temperatures.

temperature. According to the characteristic MEL traces in Fig. S7 within the Supplemental Material [11], the slowly declining HFE of dev 2 at 20 K is attributed to the B-suppressed TTA process. Similar to the temperature-dependent HFEs of dev 2, the HFE of dev 1 converts from a slow rise to a quick saturation as the temperature decreases from 300 to 20 K. Although dev 1 does not present the slowly declining HFE at 20 K, we consider that its temperature-dependent HFEs are also induced by the enhanced TTA process. Slowly declining HFEs can be observed from dev 2 rather than dev 1 because the B-suppressed TQA process presents slowly increasing HFEs and TQA in dev 2 is weaker than that in dev 1 at same bias currents and temperatures, as shown in Figs. S9(b) and S10(b) within the Supplemental Material [11]. Furthermore, TTA happens in dev 1 and dev 2 rather than RD. This is because exciton and exciplex states coexist in dev 1 and dev 2, but there are no excitons and only exciplexes exist in RD, as exhibited in Fig. S8(b) within the Supplemental Material [11]. It is well reported that T_1 excitons can undergo the TTA process, whereas EX_3 states hardly participate in TTA [26]. This is because TTA from T_1 needs only the interaction between two neighboring molecules, but that from EX_3 requires interactions among several neighboring molecules.

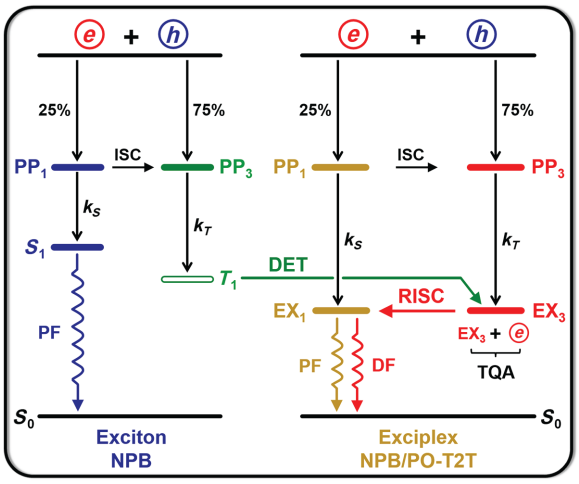

FIG. 8. Formation and evolution mechanisms of spin-pair states in dev 1 and dev 2.

To quantitatively analyze the temperature-dependent ISC, RISC, TQA, and TTA processes in dev 1 and dev 2, and ISC, RISC, and TQA in RD, the temperature-dependent MEL traces of dev 1 and dev 2 are fitted by Eq. (3) [24], while those of RD are fitted by Eq. (2).

$$\mathrm{MEL} = C_4\frac{B^2}{B^2+B_4^2} - C_5\frac{B^2}{B^2+B_5^2} + C_6\frac{B^2}{(|B|+B_6)^2} + C_7\left[A_1\frac{B^2}{B^2+B_7^2} - A_2\frac{B^2}{(|B|+B_8)^2}\right]. \quad (3)$$

In Eq. (3), the four terms model ISC, RISC, TQA, and TTA processes; B_4 (∼5 mT), B_5 (∼10 mT), B_6 (∼100 mT), B_7 (∼5 mT), and B_8 (∼100 mT) are the characteristic scales of B for ISC, RISC, TQA, and low- and high-field effects of TTA; and C_4, C_5, C_6, and C_7 are prefactors for describing the occurrence magnitudes of ISC, RISC, TQA, and TTA, respectively. As shown in Figs. 7(a)–7(c), the fitted curves (white solid lines) are very consistent with the experimental data of dev 1, dev 2, and RD. Prefactors for describing the occurrence magnitudes of ISC, RISC, TQA, and TTA processes in dev 1 and dev 2 and ISC, RISC, and TQA in RD at different temperatures are summarized in Figs. 7(d) and S10 within the Supplemental Material [11], respectively. Obviously, the TTA processes in dev 1 and dev 2 have same temperature dependencies, which enhance as the temperature decreases. This is because the lifetimes of T_1 excitons are prolonged at low temperature due to their reduced nonradiative transitions [26]. As for the ISC and TQA processes in dev 1, dev 2, and RD, they also display the same temperature dependencies. Specifically, ISC processes in these three devices weaken with decreasing temperature since ISC is an endothermic process [27]. In addition, TQA processes in these three devices weaken with decreasing temperature owing to the reduced mobility of charge carriers [26]. Although ISC and TQA in dev 1, dev 2, and RD have the same temperature dependencies, the RISC processes in these three devices show different temperature dependencies [Fig. 7(d)]. Specifically, RISC in dev 1 displays the nonmonotonic change that first enhances and then weakens as the temperature decreases, whereas those in dev 2 and RD weaken monotonically. These different temperature-dependent RISC processes are interpreted in detail in Fig. 8.

E. Microscopic physical processes of spin-pair states in dev 1, dev 2, and RD

To help understand the evolution processes of exciton and exciplex states and the formation mechanisms of MEL traces from dev 1, dev 2, and RD, microscopic physical processes occurring in dev 1 and dev 2 are shown in Fig. 8 and those occurring in RD are displayed in Fig. S11 within the Supplemental Material [11]. As can be seen, holes and electrons injected from their own electrodes first recombine under Coulomb attraction and then form weakly bound PP_1 and PP_3 on separate molecules (i.e., intermolecular electron-hole pairs) [31–33]. PP_1 and PP_3 can interconvert via the ISC and RISC processes because PP_1 and PP_3 are nearly degenerate in energy and spin flipping can be achieved by the hyperfine interaction (HFI) on the scale of several millitesla [31–35]. Next, PP_1 and PP_3 in exciton-based OLEDs further evolve into strongly bound S_1 and T_1 on the single molecule (i.e., intramolecular electron-hole pairs) with their rate constants of k_S and k_T [24,27]. Unlike intermolecular PP_1 and PP_3, intramolecular S_1 and T_1 cannot interconvert because the energy gap between S_1 and T_1 is far larger than that corresponding to HFI [24,27]. Although the ISC and RISC processes between PP_1 and PP_3 occur simultaneously, the interconversion of PP states is often dominated by the ISC from PP_1 to PP_3 (PP ISC, $PP_1 \rightarrow PP_3$) because k_T is usually larger than k_S [31]. When an external B is present, the Zeeman effect splits the energy levels of degenerated PP_3 ($PP_{3,0}$, $PP_{3,+}$, $PP_{3,-}$) [32], as shown in Fig. S12 within the Supplemental Material [11]. Although PP_1 can still convert into $PP_{3,0}$ because of the small spin-exchange energy, PP_1 cannot convert into $PP_{3,+}$ and $PP_{3,-}$ owing to the large one. This leads to the B-suppressed PP ISC and the increased quantity of PP_1 [31]. Because the increased PP_1 evolve into S_1, the quantity of S_1 rises. This quickly enhances the device EL intensity within the narrow range of the hyperfine field, i.e., a sharply increasing LFE of the MEL curve (the inverted Lorentzian line shape) is obtained within the field range of several millitesla, as shown by the fingerprint black line in Fig. S7 within the Supplemental Material [11].

Unlike PP states in exciton-based OLEDs, PP_1 and PP_3 in exciplex-based OLEDs further evolve into weakly bound EX_1 and EX_3 on distinct molecules [36,37]. EX_1 and EX_3 can also interconvert via the ISC and RISC processes under the HFI because EX_1 and EX_3 are intrinsically intermolecular excited states and almost degenerate in energy [24,33]. Note that the interconversion of EX states is often governed by the RISC from EX_3 to EX_1 (EX RISC, $EX_3 \rightarrow EX_1$). This is because the quantity of EX_3 is 3 times that of EX_1 and the lifetime of EX_3 (around 10^{-6} s) is 3 orders of magnitude longer than that of EX_1 (around 10^{-9} s) [19,33]. Furthermore, EX-RISC is also suppressed by the external B owing to the lift of degenerated EX_3 ($EX_{3,0}$, $EX_{3,+}$, $EX_{3,-}$) by Zeeman splitting [24,38], as displayed in Fig. S12 within the Supplemental Material [11]. When EX RISC is suppressed by the external B, the quantity of EX_1 decreases, meaning that the device EL intensity rapidly weakens within the narrow range of the hyperfine field, i.e., a quickly declining LFE of the MEL curve (the upright Lorentzian line shape) is obtained within the field range of several millitesla, as shown by the fingerprint red line in Fig. S7 within the Supplemental Material [11]. In

addition to EX RISC, EX_3 interacts with excessive charge carriers [38,39], i.e., the TQA process happens. As for the HFE of the MEL curve induced by the *B*-suppressed TQA, it is explained in detail in Text S3 within the Supplemental Material [11]. Based on these descriptions of the *B*-mediated PP ISC and EX RISC, it can be concluded that the LFE of the MEL trace is determined by the superposition of the positive LFE from *B*-mediated PP ISC and the negative LFE from *B*-mediated EX RISC.

As shown in Fig. 6(c), LFEs of RD are dominated by the *B*-suppressed PP ISC, i.e., EX RISC is weaker than PP ISC. This is because the HFEs of RD indicate that the TQA process ($\vec{e} + EX_3 \rightarrow e\downarrow + S_0$) occurs in the device and TQA weakens EX RISC by reducing the number of EX_3 (Fig. S11 in the Supplemental Material [11]). Theoretically, EX RISC cannot be observed from the MEL traces of dev 1 and dev 2, since the TQA process also occurs in these two devices. However, the opposite experimental results are obtained, i.e., EX RISC can be observed from the IFEs of dev 1 and dev 2 [Figs. 6(a) and 6(b)]. This is because the DET channel from T_1 to EX_3 ($T_1 \rightarrow EX_3$) exists in dev 1 and dev 2 (Figs. 8 and S13 in the Supplemental Material [11]) owing to the close energies of T_1 (around 2.3 eV) [40] and EX_3 (around 2.1 eV) calculated from the exciplex-emission peak in the device EL spectra [Fig. 1(e)]. In addition, DET can increase the quantity of EX_3 and therefore enhance EX RISC from EX_3 to EX_1 ($EX_3 \rightarrow EX_1$). This DET channel has not been previously discovered in PHJ OLEDs and it is further proved by analyzing PL characteristics of the NPB, PO-T2T, and NPB:PO-T2T films as described in Text S4 and Fig. S14 within the Supplemental Material [11]. As for RD, it has no IFEs. This is because the DET channel does not exist in RD, since there are no excitons and only exciplexes are present in RD, which can be proved by there being only exciplex emissions in its EL spectra, as displayed in Figs. S8(b) and S11 within the Supplemental Material [11]. Furthermore, note that the characteristic scale of *B* (around 10 mT) for EX RISC facilitated by the DET channel is larger than that (about 5 mT) for the conventional EX RISC. This is because the characteristic scale of *B* for EX RISC rises with decreasing spatial extension of EX states [31] and the spatial extension of EX states generated by DET is smaller than that of traditional EX states formed by electron-hole recombination (Fig. S15 in the Supplemental Material [11]). Specifically, the exciton radius of EX states generated by DET is less than 10 Å since the electron-exchange distance of DET is smaller than 10 Å [41], but the exciton radius of EX states formed by the electron-hole recombination is usually 10 Å [42].

According to the current-dependent EL spectra from dev 1 and dev 2 at different temperatures (Figs. 2 and 3), the numbers of T_1 excitons in these two devices have various current and temperature dependencies. This indicates that different current- and temperature-dependent DET and EX RISC processes happen in dev 1 and dev 2. As shown in Fig. 6(d), EX RISC in dev 1 enhances with increasing bias current, whereas that in dev 2 weakens. These two opposite current dependencies of EX RISC can be explained by analyzing different current-dependent competitions between TQA and DET in dev 1 and dev 2. As shown in Fig. S9(b) within the Supplemental Material [11], the TQA processes in dev 1 and dev 2 have same current dependencies, which enhance with increasing bias current. However, current-dependent EL spectra of dev 1 and dev 2 reflect that the DET channels in these two devices have different current dependencies. Specifically, the EL spectra of dev 1 indicate that the quantity of T_1 excitons in dev 1 rises with increasing bias current, whereas those of dev 2 reflect that the number of T_1 excitons in dev 2 is insensitive to the bias current. That is, the DET in dev 1 enhances as the bias current increases, whereas that in dev 2 hardly changes. Based on these discussions of current-dependent TQA and DET in dev 1, we consider that current-dependent EX RISC in dev 1 is dominated by its current-dependent DET. This is because EX RISC can be observed from IFEs of dev 1 owing to the presence of the DET channel and the DET changes significantly with the bias current. Although DET also exists in dev 2, it hardly changes with the bias current. This reflects that the current-dependent EX RISC in dev 2 is governed by its current-dependent TQA. Thus, EX RISC in dev 1 enhances as the bias current increases, whereas that in dev 2 weakens [Fig. 6(d)].

Moreover, EX RISC in dev 1 and dev 2 show nonmonotonic and monotonic temperature dependencies, respectively [Fig. 7(d)]. Specifically, EX RISC in dev 1 first enhances and then weakens as the temperature decreases, but that in dev 2 always weakens. These two distinct temperature dependencies of EX RISC are induced by different temperature-dependent competitions between TQA and DET in dev 1 and dev 2. Although the TQA processes in dev 1 and dev 2 have the same temperature dependencies, which weaken with decreasing temperature, as exhibited in Fig. S10(b) within the Supplemental Material [11], their temperature-dependent EL spectra indicate that the DET channels in these two devices have different temperature dependencies. Specifically, the EL spectra of dev 1 indicate that the quantity of T_1 excitons in dev 1 first rises but then reduces as the temperature decreases, whereas those of dev 2 reflect that the number of T_1 excitons in dev 2 reduces monotonically. That is, DET in dev 1 first enhances and then weakens with decreasing temperature, whereas that in dev 2 always weakens. We consider that temperature-dependent EX RISC in dev 1 and dev 2 are determined by their temperature-dependent DET. This is because EX RISC processes in these two devices are facilitated by the DET channel and their DETs have significant temperature dependencies. Hence, EX RISC in dev 1 first enhances and then weakens as the temperature decreases, but that in dev 2 weakens monotonically [Fig. 7(d)]. Obviously,

we use MEL to discover various current- and temperature-dependent DET channels between exciton and exciplex states in dev 1 and dev 2 via analyzing different current and temperature dependencies of EX RISC processes in these two devices.

IV. CONCLUSION

In summary, unreported competitions between NPB exciton and NPB/PO-T2T exciplex emissions and an undiscovered DET channel from triplet NPB excitons to triplet NPB/PO-T2T exciplex states are discussed by measuring current- and temperature-dependent EL spectra and MEL traces from NPB/PO-T2T PHJ OLEDs with different hole-injection abilities. The R of I_{exciton} to I_{exciplex} from the device with a poor hole-injection ability hardly changes with the bias current at each temperature and reduces monotonically as the temperature decreases at each bias current. Surprisingly, the R from the device with a good hole-injection ability rises with increasing bias current at all temperatures and shows nonmonotonic variation, which first rises and then reduces with decreasing temperature at each bias current. These rich current- and temperature-dependent competitions between exciton and exciplex emissions are caused by distinct current and temperature dependencies of the electron-tunneling effects occurring at the NPB/PO-T2T interfaces of the devices with different hole-injection abilities. More surprisingly, MEL is used as a fingerprint probing tool to discover that the DET channel from T_1 to EX_3 exists in these devices and DET can enhance the EX RISC process from EX_3 to EX_1, which cannot be found by the usual detection technique of EL spectra. Owing to different current and temperature dependencies of the numbers of T_1 excitons in these devices, various current- and temperature-dependent DET and RISC processes happen, which induce abundant MEL behaviors. Evidently, this work presents insights into the competition and DET processes between exciton and exciplex states in PHJ OLEDs.

ACKNOWLEDGMENTS

We acknowledge financial support from the Natural Science Foundation of China (Grants No. 11874305 and No. 11374242).

[1] K. Leitonas, M. Guzauskas, U. Tsiko, J. Simokaitiene, D. Volyniuk, and J. V. Grazulevicius, White vertical organic permeable-base light-emitting transistors obtained by mixing of blue exciton and orange interface exciplex emissions, J. Mater. Chem. C **10**, 9786 (2022).

[2] M. Carvelli, A. van Reenen, R. A. J. Janssen, H. P. Loebl, and R. Coehoorn, Exciton formation and light emission near the organic-organic interface in small-molecule based double-layer OLEDs, Org. Electron. **13**, 2605 (2012).

[3] Y. Y. Hao, W. X. Meng, H. X. Xu, H. Wang, X. G. Liu, and B. S. Xu, White organic light-emitting diodes based on a novel Zn complex with high CRI combining emission from excitons and interface-formed electroplex, Org. Electron. **12**, 136 (2011).

[4] F. J. Zhang, S. L. Zhao, D. W. Zhao, W. W. Jiang, Y. Li, G. C. Yuan, H. N. Zhu, and Z. Xu, Electroplex emission from bi-layer blue emitting organic materials, Phys. Scr. **75**, 407 (2007).

[5] S. J. He, D. K. Wang, N. Jiang, J. S. Tse, and Z. H. Lu, Tunable excitonic processes at organic heterojunctions, Adv. Mater. **28**, 649 (2016).

[6] Y. Nishikitani, N. Inokuchi, H. Nishide, S. Uchida, T. Shibanuma, and S. Nishimura, Effect of π-conjugated polyelectrolyte on performance of white polymer light-emitting diodes based on excitons and exciplexes having long intermolecular distances, J. Phys. Chem. C **120**, 13976 (2016).

[7] S. Y. Yang, X. L. Zhang, Z. D. Lou, and Y. B. Hou, Charge tunneling and cross recombination at organic heterojunction under electric fields, Eur. Phys. J. B **59**, 151 (2007).

[8] H. J. Ji and J. G. Jang, White organic light-emitting diode using the exciplex between DNTPD and ET-137, Mol. Cryst. Liq. Cryst. **563**, 223 (2012).

[9] M. Zhang, C. J. Zheng, H. Lin, and S. L. Tao, Thermally activated delayed fluorescence exciplex emitters for high-performance organic light-emitting diodes, Mater. Horiz. **8**, 401 (2021).

[10] H. B. Kim and J. J. Kim, Diffusion Mechanism of Exciplexes in Organic Optoelectronics, Phys. Rev. Appl. **13**, 024006 (2020).

[11] See the Supplemental Material at http://link.aps.org/supplemental/10.1103/PhysRevApplied.19.054067 for additional data descriptions of prefactors used to describe the occurrence magnitudes of the ISC, TQA, and TTA processes in dev 1 and dev 2, and energy-level structures and photoelectric properties of dev 3 and RD.

[12] W. Y. Hung, G. C. Fang, S. W. Lin, S. H. Cheng, K. T. Wong, T. Y. Kuo, and P. T. Chou, The first tandem, all-exciplex-based WOLED, Sci. Rep. **4**, 5161 (2014).

[13] J. K. Yuan, X. M. Guo, W. Liu, Y. F. Dai, Q. Sun, D. Z. Yang, X. F. Qiao, and D. G. Ma, Investigation on the mechanism of charge generation in organic heterojunctions: Analysis of I-V and C-V characteristics, Org. Electron. **88**, 105979 (2021).

[14] H. Cruz, A. Hernández-Cabrera, and A. Muñoz, Resonant tunnelling of electrons through parabolic quantum wells: An analytical calculation of the transmission coefficient, Semicond. Sci. Technol. **6**, 218 (1991).

[15] V. I. Egorkin, M. N. Zhuravlev, and V. V. Kapaev, Electron transport simulation in resonant-tunneling GaN/AlGaN heterostructures, Semiconductors **45**, 1638 (2011).

[16] Sim4tec GmbH, <www.sim4tec.com>.

[17] R. A. Prada and A. M. A. Vargas, Optimization of the host–guest system within an OLED using different models of mobility, Phys. B **455**, 85 (2014).

[18] A. C. Morteani, P. K. H. Ho, R. H. Friend, and C. Silva, Electric field-induced transition from heterojunction to bulk

charge recombination in bilayer polymer light-emitting diodes, Appl. Phys. Lett. **86**, 163501 (2005).

[19] Q. M. Peng, A. W. Li, Y. X. Fan, P. Chen, and F. Li, Studying the influence of triplet deactivation on the singlet-triplet interconversion in intra-molecular charge-transfer fluorescence-based OLEDs by magneto-electroluminescence, J. Mater. Chem. C **2**, 6264 (2014).

[20] Y. W. Xu, X. M. Liang, X. H. Zhou, P. S. Yuan, J. D. Zhou, C. Wang, B. B. Li, D. H. Hu, X. F. Qiao, X. F. Jiang, L. L. Liu, S. J. Su, D. G. Ma, and Y. G. Ma, Highly efficient blue fluorescent OLEDs based on upper level triplet-singlet intersystem crossing, Adv. Mater. **31**, 1807388 (2019).

[21] V. Jankus, C. Winscom, and A. P. Monkman, Dynamics of triplet migration in films of *N*,*N*(-diphenyl-*N*,*N*(-bis(1-naphthyl)-1, 1(-biphenyl-4, 4(-diamine, J. Phys. Condens. Matter **22**, 185802 (2010).

[22] C. S. Redondo, P. Kleine, K. Roszeitis, T. Achenbach, M. Kroll, M. Thomschke, and S. Reineke, Interplay of fluorescence and phosphorescence in organic biluminescent emitters, J. Phys. Chem. C **121**, 14946 (2017).

[23] Y. Q. Hu, X. T. Tang, R. H. Pan, J. Q. Deng, H. Q. Zhu, and Z. H. Xiong, Spin-pair state-induced exceptional magnetic field responses from a thermally activated delayed fluorescence-assisted fluorescent material doping system, Phys. Chem. Chem. Phys. **21**, 17673 (2019).

[24] J. Xu, X. T. Tang, X. Zhao, H. Q. Zhu, F. L. Qu, and Z. H. Xiong, Abnormal Reverse Intersystem Crossing of Polaron-Pair States and Its Conversion to Intersystem Crossing via the Regulation of Intermolecular Electron-Hole Spacing Distance, Phys. Rev. Appl. **14**, 024011 (2020).

[25] Y. F. Wang, K. S. Tiras, N. J. Harmon, M. Wohlgenannt, and M. E. Flatté, Immense Magnetic Response of Exciplex Light Emission due to Correlated Spin-Charge Dynamics, Phys. Rev. X **6**, 011011 (2016).

[26] J. Xiang, Y. B. Chen, W. Y. Jia, L. X. Chen, Y. L. Lei, Q. M. Zhang, and Z. H. Xiong, Realization of triplet-triplet annihilation in planar heterojunction exciplex-based organic light-emitting diodes, Org. Electron. **28**, 94 (2016).

[27] X. T. Tang, R. H. Pan, H. Q. Zhu, X. Zhao, L. Y. Tu, and Z. H. Xiong, The origin of interlayer-induced significant enhancement of EQE in CzDBA-based OLEDs studied by magneto-electroluminescence, Appl. Phys. Lett. **118**, 013503 (2021).

[28] Ö Mermer, G. Veeraraghavan, T. L. Francis, Y. Sheng, D. T. Nguyen, M. Wohlgenannt, A. Köhler, M. K. Al-Suti, and M. S. Khan, Large magnetoresistance in nonmagnetic π-conjugated semiconductor thin film devices, Phys. Rev. B **72**, 205202 (2005).

[29] S. Inal, M. Schubert, A. Sellinger, and D. Neher, The relationship between the electric field-induced dissociation of charge transfer excitons and the photocurrent in small molecular/polymeric solar cells, J. Phys. Chem. Lett. **1**, 982 (2010).

[30] S. A. Bagnich, U. Niedermeier, C. Melzer, W. Sarfert, and H. von Seggern, Electron-hole pair mechanism for the magnetic field effect in organic light emitting diodes based on poly(paraphenylene vinylene), J. Appl. Phys. **106**, 113702 (2009).

[31] S. A. Crooker, F. Liu, M. R. Kelley, N. J. D. Martinez, W. Nie, A. Mohite, I. H. Nayyar, S. Tretiak, D. L. Smith, and P. P. Ruden, Spectrally resolved hyperfine interactions between polaron and nuclear spins in organic light emitting diodes: Magneto-electroluminescence studies, Appl. Phys. Lett. **105**, 153304 (2014).

[32] F. Liu, M. R. Kelley, S. A. Crooker, W. Nie, A. D. Mohite, P. P. Ruden, and D. L. Smith, Magnetoelectroluminescence of organic heterostructures: Analytical theory and spectrally resolved measurements, Phys. Rev. B **90**, 235314 (2014).

[33] P. Janssen, M. Cox, S. H. W. Wouters, M. Kemerink, M. M. Wienk, and B. Koopmans, Tuning organic magnetoresistance in polymer-fullerene blends by controlling spin reaction pathways, Nat. Commun. **4**, 2286 (2013).

[34] W. Ratzke, S. Bange, and J. M. Lupton, Direct Detection of Singlet-Triplet Interconversion in OLED Magnetoelectroluminescence with a Metal-Free Fluorescence-Phosphorescence Dual Emitter, Phys. Rev. Appl. **9**, 054038 (2018).

[35] R. Geng, R. C. Subedi, H. M. Luong, M. T. Pham, W. C. Huang, X. G. Li, K. Hong, M. Shao, K. Xiao, L. A. Hornak, and T. D. Nguyen, Effect of Charge Localization on the Effective Hyperfine Interaction in Organic Semiconducting Polymers, Phys. Rev. Lett. **120**, 086602 (2018).

[36] T. Basel, D. Sun, S. Baniya, R. McLaughlin, H. Choi, O. Kwon, and Z. V. Vardeny, Magnetic field enhancement of organic light-emitting diodes based on electron donor-acceptor exciplex, Adv. Electron. Mater. **2**, 1500248 (2016).

[37] M. S. Wang, H. S. Shin, F. Zhou, H. X. Xu, P. Prabhakaran, B. Dryzhakov, H. B. Su, K. S. Lee, and B. Hu, Identifying different spin mixing channels occurring in charge-transfer states, J. Phys. Chem. C **124**, 14832 (2020).

[38] L. Y. Tu, X. T. Tang, Y. Wang, X. Zhao, C. H. Ma, S. N. Ye, and Z. H. Xiong, Dynamic Behaviors of Exciplex States in Rubrene/C_{60}-based OLEDs with Sub-Band-Gap Turn-On Electroluminescence, Phys. Rev. Appl. **16**, 064002 (2021).

[39] C. G. Zhao, F. G. Zhao, K. Wang, H. M. Yu, T. Y. Huang, R. Wang, C. X. Zhang, B. Hu, and L. Duan, Stabilization of Blue Emitters with Thermally Activated Delayed Fluorescence by the Steric Effect: A Case Study by Means of Magnetic Field Effects, Phys. Rev. Appl. **14**, 034059 (2020).

[40] Y. P. Wang, W. J. Wang, Z. J. Huang, H. H. Wang, J. T. Zhao, J. H. Yu, and D. G. Ma, High-efficiency red organic light-emitting diodes based on double-emissive layer with the external quantum efficiency over 30%, J. Mater. Chem. C **6**, 7042 (2018).

[41] C. H. Chen, W. C. Ding, B. Y. Lin, J. J. Huang, M. K. Leung, J. H. Lee, and T. L. Chiu, Long-distance triplet diffusion and well-packing hosts with ultralow dopant concentration for achieving high-efficiency TADF OLED, Adv. Opt. Mater. **9**, 2100857 (2021).

[42] Z. Shen, P. E. Burrows, S. R. Forrest, M. Ziari, and W. H. Steier, Electroabsorption due to excitons in crystalline molecular thin films grown by organic molecular beam deposition, Chem. Phys. Lett. **236**, 129 (1995).